Phase-Stabilized Side-Branch RoF Link for Extensible Frequency Dissemination in Distributed Systems

Zhongze Jiang, Feifei Yin, Yitang Dai, Tianpeng Ren, and Kun Xu, *Member, IEEE*

***Abstract*—Synchronization is a long-standing challenge in modern large-scale distributed systems, and newly deployed systems such as 5G and modern netted radars require more extensive synchronization. As the number of distributed stations increasing, new synchronization solution with much effort on extensibility is highly expected. In this paper we first analyze the requirements on extensibility of fiber-based sync systems, and then propose a phase-stabilized side-branch radio-over-fiber (RoF) link, which fully satisfies the extensibility requirements. The extensible side-branch link can be constructed at any intermediate point along the main link, without any reconfiguration at the central station, which is especially feasible when adding extra stations in system capacity expansion. The main link phase shift is first stabilized by tuning the optical carrier wavelength, while another phase-locked-loop constructed at the starting point of the branch link stabilizes the phase shift from the central station to the end of branch link, by phase locking two phase-varying signals. Moreover, the phase-stable side branch is inherently extensible to multiple frequency signals, which can be used in receivers requiring multiple local oscillators (LOs). Two frequency signals are simultaneously disseminated to the end of branch link in the experiment, with frequency stability optimization of two orders of magnitude on both LOs achieved. The proposed stable side-branch RoF link shows the potential of constructing a highly-extensible frequency dissemination network for the synchronization in modern distributed systems.**

***Index Terms*—Frequency synchronization, extensible side-branch, distributed systems, radio-over-fiber.**

I. Introduction

FREQUENCY synchronization is the key enabling technology in modern large-scale distributed information systems and applications like time-sensitive networking for 5G fronthaul and backhaul [1]–[4], indoor/outdoor positioning [5], [6], carrier recovery in optical communications [7], [8], heterodyne receivers in coherently netted radars and radio telescopes [9]–[12], and data center interconnections [13], [14], etc., where the disseminated and recovered frequency signals are usually essential either for carrier (local oscillator, LO) synchronization [6]–[11] or for precise and fine-grained time control [2], [13]. The required synchronization accuracy can be at sub-nanosecond level or beyond [1], [5], for decimeter/centimeter positioning, etc. The conventional synchronizing solution using the Global Navigation Satellite System (GNSS) may become insufficient and expensive, due to the coverage scenarios being dramatically increased in the 5G and other future networks [15], [16]. In addition, the reliability of synchronization network is also highly required to deal with the potential sync degradation caused by failure or attack [11], [17]. Due to the advantages of low transmission loss, large bandwidth, anti-electromagnetic interference and high reliability, deploying ground-based synchronization network over optical fiber links has been considered as a crucial part of infrastructure in the next-generation distributed information systems.

Researches on stable frequency dissemination and synchronization in optical fiber can be traced back to the early 1990s, with several pioneering researches accomplished decades ago [18], [19]. From a historical perspective of the development of this technology, the point-to-point optical fiber links for delivering frequency signals have been firstly proposed [19]–[22], and most of them are based on phase compensation assisted by the round-trip signal, either passively [19], [20] or actively [21], [22]. As the number of remote stations sharply increasing in applications (e.g., in the squared kilometer arrays), different one-to-multipoint time and frequency delivery schemes have been proposed—the extensibility of synchronization system has been taken into consideration [23]–[28]. Unlike the GNSS-based synchronization, which is inherently capable of broadcasting time and frequency to multiple users, it is much harder for the ground-based sync system like optical fiber links to disseminate frequency to multiple locations. In principle, the one-to-multipoint fiber-based sync schemes employ either a bus topology [23]–[25] or a ring-form topology [26]–[28], and the frequency stabilization at recovery points mainly relies on phase conjugation of the signals received in two different directions (i.e., forward v.s. backward, clockwise v.s. counter-clockwise). Apart from the bus-topology and ring-form one-to-multipoint solutions, it has been realized by researchers that constructing

Manuscript received July 27, 2021; revised September 13, 2021; accepted September 15, 2021. Date of publication September 20, 2021; date of current version October 7, 2021. This work was supported in part by the National Key Research and Development Program of China under Grant 2018YFA0701902, in part by the National Natural Science Foundation of China under Grants 61625104, 62071055, 61821001, and 61801037, in part by ZTE Industry-Academia-Research Cooperation Funds. *(Corresponding author: Feifei Yin.)*

Zhongze Jiang, Feifei Yin, Yitang Dai, and Kun Xu are with the State Key Laboratory of Information Photonics and Optical Communications, Beijing University of Posts and Telecommunications, Beijing 100876, China (e-mail: zbupt@bupt.edu.cn; yinfeifei@bupt.edu.cn; ytdai@bupt.edu.cn; xukun@bupt.edu.cn).

Tianpeng Ren is with the Science and Technology on Aerospace Flight Dynamics Laboratory, Beijing Aerospace Control Center, Beijing 100094, China (e-mail: tpren@nudt.edu.cn).

Digital Object Identifier 10.1109/JPHOT.2021.3113663

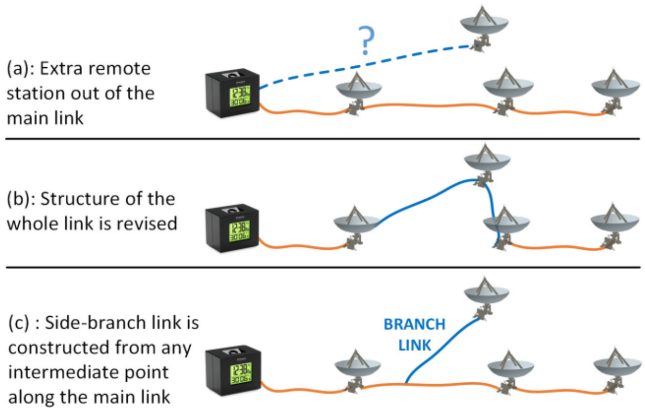

Fig. 1. Different link topology designs when an extra remote station is added. A branch link topology allows the extension of new remote sites without modification of the currently-running synchronization link, wheras the challenge remains in the synchronization of branch link.

a frequency dissemination network with branch topology may have unique advantage. Fig. 1 illustrates this side-branch synchronization concept. The crucial point is that when an extra remote station is added (which is common in system upgrading and capacity expansion), the whole link structure of the bus or ring-form system has to be modified to be compatible with the extra sites (Fig. 1(b)), whereas one does not have to revise the structure of the already–constructed synchronization link when adopting the side-branch topology (Fig. 1(c)). This feature makes the branch-link synchronization option especially convenient for dealing with the ever-increasing number of distributed stations.

The primary challenge of the side-branch frequency dissemination remains stabilizing the phase shift or time delay from the central station to any remote end of the branch link. Only a few branch-topology frequency transfer schemes have been proposed in recent years, for either optical or radio frequencies [29]–[31]. Phase-conjugation-based passive phase correction at the remote end of the branch link is still widely employed. However, like the passive phase compensation methods used in the point-to-point and one-to-multipoint structures, it is still hard to transfer more than one frequency signal and passively compensate their phase error in one set of configuration (i.e., different frequencies must be compensated separately). Actually, to remove residual spurious components so as to prevent reception interference at the remote antenna, multiple LO signals are generally used to down-convert the RF signal [11], [12]. Traditional way is to deliver one reference signal to remote sites to synchronize multiple oscillators or to generate multiple LOs by frequency multipliers. In both ways, varying phase perturbations in associated electronics must be accounted for. An attractive way is to generate multiple LOs in the central station and deliver them to different remote sites with coherent phases, which will reduce the complexity of electronics at each remote end. Therefore, the extensibility of state-of-the-art fiber-based frequency sync systems can be evaluated mainly in two aspects—(1), the extensibility of disseminating to multiple locations and the compatibility when adding extra remote sites; (2), the extensibility of disseminating multiple LOs simultaneously.

In this paper, we present a phase-stabilized side-branch radio-over-fiber (RoF) link that simultaneously disseminates different frequencies to the end of the branch link, which satisfies both of the above requirements on synchronization extensibility. The branch link can be installed at any point along the main link and works independently, without any structural or functional changes in the central station. The phase shift on the main link is firstly locked by a feedback algorithm tuning the optical carrier wavelength at the central station. Then the branch link phase error compensation works at the starting point of the branch link, by phase locking two signals whose phases are all time-varying with respect to the signal source. More than one stable local oscillator can be simultaneously disseminated to the end of the side-branch link, or to different branch links. Two LOs at different frequencies are coherently transferred to the remote end of the branch link in the experiment, and the frequency stability of the recovered LOs can be optimized by two orders of magnitude.

II. Principle of Side-Branch Frequency Dissemination

A schematic of the proposed extensible side-branch RoF link for multiple frequency dissemination is illustrated in Fig. 2. The side-branch frequency dissemination system consists of one main link and one or more branch links, and the system aims to disseminate one or more local oscillators from the central station to the end of the branch link.

At the central station, the local oscillator LO_1 to be transferred through the link (with the angular frequency of ω_1) is electro-optically converted by a Mach-Zehnder modulator (MZM), with the optical carrier generated by a wavelength tunable laser (WTL_1). The optical signal after intensity modulation first passes through an optical circulator (CIR), and is transferred through the main link to the remote end. At the remote end of the main link, a portion of the optical power is reflected by a Faraday rotation mirror (FRM), and then transferred back to the central station along the main link. The round-trip signal is opto-electrically converted by a photodetector (PD), and extracted by a band-pass filter (BPF_1). The fiber link suffers from delay fluctuations mainly caused by temperature variations and sometimes mechanical stress. At the central station, the phase difference between the original LO_1 and the round-trip LO_1 is measured by a phase detector, the result of which is then digitized and fed into a feedback algorithm (running on a micro control unit, MCU) to alter the carrier wavelength. Different feedback algorithms can be applied to adjust wavelength, including the most widely used proportion-integral-derivative (PID) feedback. Taking advantage of the fiber chromatic dispersion, the feedback algorithm continuously alters the wavelength, resulting in a dispersion-induced fiber delay change used to counteract the phase shift caused by environmental variations [32]. Therefore, the phase shift of LO_1 is first locked in the main link, both single-trip and round-trip.

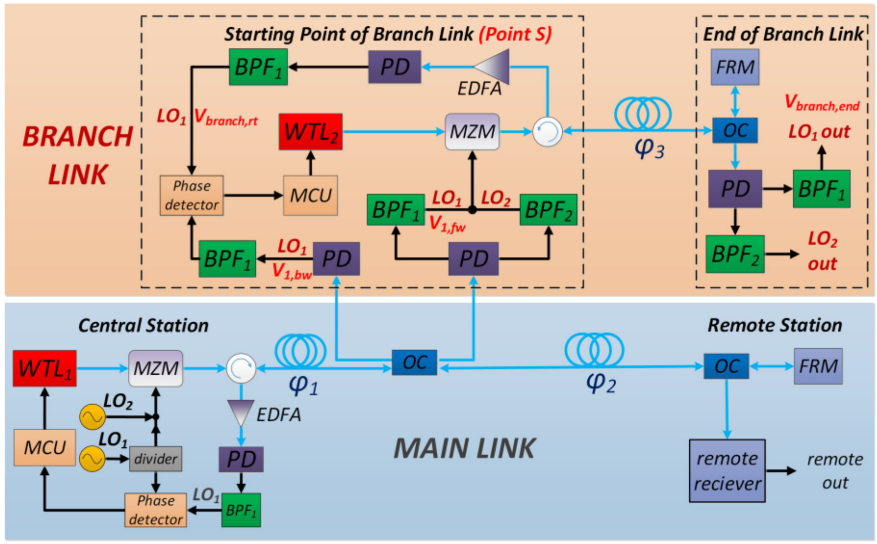

Fig. 2. Principle and experimental setup of the extensible side-branch RoF link for multiple frequency dissemination. The side-branch RoF link can be constructed at any intermediate point along the main link, without any reconfiguration at the central station. WTL, wavelength tunable laser. MZM, Mach-Zehnder modulator. PD, photodetector. OC, optical coupler. CIR, optical circulator. FRM, Faraday rotation mirror. EDFA, erbium-doped fiber amplifier. BPF, electric band-pass filter. MCU, micro control unit.

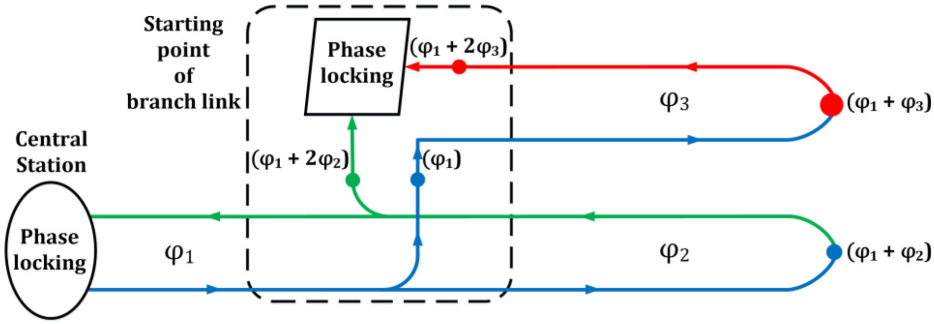

Fig. 3. Phase relationships in the main and branch fiber link. The phase values without parenthesis denote the phase shift in a particular segment of fiber link; the phase values within the parentheses denote the phase shift at specific point with respect to the signal source in the central station.

The branch link can be constructed from any intermediate point along the main link, without any reconfiguration at the central station. A 2×2 optical coupler is installed at the starting point of the branch link (i.e., Point S in Fig. 2) to couple out both the forward and backward optical signals from the main link, followed by photodetectors and band-pass filters to extract the electric signals of both directions, as is illustrated in Fig. 2. To disseminate the frequency signal into the branch link, the recovered forward electric signal (i.e., $V_{1,fw}$) are again electro-optically converted by the MZM at point S, with the optical carrier generated by another wavelength tunable laser (WTL_2). Similar to the signal path in the central station, the modulated optical signal at point S is injected into the fiber branch link. When reaching the remote end of the branch link, a part of the optical power is also reflected backward by an FRM, with the other part of optical power left for electric signal recovery. The backward optical signal in the branch link is opto-electrically converted by a PD at the starting point of branch link.

The side-branch link phase stabilization works as follows, and Fig. 3 helps illustrate the phase relationships at different points in the main & branch link. Let the total phase shift of LO_1 between the central station and point S be φ_1, and the total phase shift between point S and the remote end of main link be φ_2. At the starting point of branch link, the forward electric signal referring to LO_1, $V_{1,fw}$, can be expressed as:

$$V_{1,fw} \propto \cos\left(\omega_1 t + \varphi_1\right), \tag{1}$$

and the corresponding backward electric signal, $V_{1,bw}$, can be expressed as:

$$V_{1,bw} \propto \cos\left(\omega_1 t + \varphi_1 + 2\varphi_2\right). \tag{2}$$

We here assume the single-trip phase shift induced by environmental factors (e.g., temperature variation, etc.) in the branch link is denoted by $\Delta\varphi_b$. A phase detector compares the phase difference between the branch round-trip signal (referring to LO_1), $V_{branch,rt}$, and the backward signal coupled out at the

starting point of branch link, $V_{1,bw}$. This phase difference is used to alter the wavelength of the WTL_2 at point S. Similar to the algorithms in the main link, when the wavelength of WTL_2 is tuned from $\lambda_{b,1}$ to $\lambda_{b,2}$, the single-trip delay difference on the branch link caused by chromatic dispersion would be:

$$\Delta\,\tau_b = \left[\int_{\lambda_{b,1}}^{\lambda_{b,2}} D_b\left(\lambda\right) d\lambda\right]\; L_b, \tag{3}$$

where L_b is the branch fiber length and $D_b(\lambda)$ is the dispersion coefficient of the branch fiber. Therefore, the round-trip electric signal in branch link after wavelength tuning is:

$$\begin{aligned} V_{branch,rt} &\propto \cos\left(\omega_1 t + \varphi_1 + 2\Delta\varphi_b + 2\omega_1\Delta\tau_b\right) \\ &= \cos\left(\omega_1 t + \varphi_1 + 2\varphi_3\right), \end{aligned} \tag{4}$$

where φ_3 denotes the total single-trip phase shift in branch link.

The key point of branch link stabilization is that the feedback algorithm at Point S (labeled in Fig. 2) is designed to compare and lock the phase difference between the round-trip signal, $V_{branch,rt}$, and the backward signal from the main link, $V_{1,bw}$. When the feedback algorithm works properly, the phase difference between the above two signals is locked to be a constant:

$$\Theta\left(V_{branch,rt}\right) - \Theta\;\left(V_{1,bw}\right) = \;2\;\left(\varphi_3 - \varphi_2\right) = \varphi_c^{'} \tag{5}$$

where φ_c' is a constant phase shift and $\Theta(\cdot)$ is the total phase operator. Equation (5) means that $(\varphi_3 - \varphi_2)$ keeps constant when the branch link is phase-locked by tuning the wavelength of WTL_2. Also note that $\varphi_1 + \;\varphi_2 = \varphi_c$ (i.e., φ_c is constant) holds when the main link is phase-locked by tuning WTL_1. Thus, when the algorithms in the main and branch link work properly, the output signal at the end of the branch link, $V_{branch,\,end}$, turns out to be:

$$\begin{aligned} V_{branch,\,end} &\propto \cos\left(\omega_1 t + \varphi_1 + \varphi_3\right) \\ &= \cos\left(\omega_1 t + \varphi_c + \tfrac{\varphi_c'}{2}\right) \end{aligned} \tag{6}$$

where φ_c and φ_c' are constants. Therefore, the recovered signal at the end of the branch link is phase-locked to the original source LO_1 at the central station, as is indicated in Eq. (6). Note that both φ_1 and φ_3 are time-varying with respect to the central station, but $\varphi_1 + \varphi_3$ is kept as a fixed phase shift when the two feedback algorithms work properly. That is to say, by phase-locking two phase-variant signals (i.e., $V_{branch,rt}$ and $V_{1,bw}$), a phase-stabilized signal can be recovered at the remote end of branch link.

The proposed side-branch RoF link is self-adaptive to simultaneously disseminating multiple local oscillators with stabilized phase referenced to the LOs in central station. In practical frequency synchronization applications, it is usually required more than one local oscillator to be transferred to the remote end, or to different remote ends. As is illustrated in Fig. 2, another local oscillator, LO_2, is combined with LO_1 and simultaneously transferred through the main & branch link. At the branch staring point in Fig. 2, splitting and recombining the two LOs again after PD seems of little necessity; however, considering the accumulated link noise and potential degree of nonlinearity when the signals arrive at this point, it might be optimal to first have the two LOs split, then purified by bandpass filters. This split-purify-combine process can provide the branch link with a cleaner LO input. Generally, there will be a delay difference of LO_1 and LO_2 when transmitting in the same fiber (after optical modulation) due to the fiber chromatic dispersion. When the optical carrier wavelengths keep altering for the phase stabilization of LO_1, the delay difference between the two LOs changes with time, which means theoretically the phase of LO_2 will suffer from a residual instability when LO_1 is phase-locked. However, it has been demonstrated in our previous related work that the amount of delay difference variation between LO_1 and LO_2 in this situation is too small to have practical impact as long as LO_1 and LO_2 are converted on the same optical carrier and transmitting through the same fiber link [32]. Therefore, Eq. (1)$\sim$(2) and Eq. (4)$\sim$(6) can all be applied to LO_2. As a consequence, the phase of LO_2 would also be stabilized at the end of the branch link. All the phase stabilization is achieved through the phase comparison and phase locking of LO_1 only, both in the main and branch link, which makes it intrinsically extensible to disseminating multiple LOs. It is also worth noting that the side-branch frequency dissemination system may have more active and passive components required in the branch link, which is the trade-off between system extensibility and cost.

III. Experiment and Results

A proof-of-concept experiment is conducted to verify the side-branch multiple-frequency dissemination capability. In the experiment, the main link is constructed by a 35-km fiber spool, with the starting point of the 25-km branch link chosen at the point after 20 km from central station. The wavelength tunable range of the laser covers the whole C band (1528$\sim$1565 nm). As we take advantage of the fiber chromatic dispersion to adjust and compensate the fiber delay fluctuations, large wavelength tunable range is expected to counteract the possible large delay variation range, so the whole 1550-nm band is used when tuning the wavelength, as long as other link components work properly at the wavelength.

To avoid the nonlinearity caused by fiber propagation effects such as Stimulated Brillouin Scattering (SBS) and Stimulated Raman Scattering (SRS), it is optimal for the optical power into fiber link to not exceed the SBS threshold, as the SBS threshold (e.g., typically $\sim$5 dBm @ 1550 nm in 50-km single mode fiber [33]) is much lower than that of SRS. In the experiment, the laser source power (into the MZMs) is 12.5 dBm, and each MZM has an insertion loss of around 5 dB and is biased at quadrature point, so the MZM output power into the fiber link is around 4.5 dBm, which is actually very close but not exceed the SBS threshold. Bi-directional couplers are employed, in which the coupling ratio (coupling loss) of the reverse direction is identical (or very close) to that of the forward direction, so the backward optical power in the main and branch link do not degrade heavily. A 50:50 bi-directional optical coupler is used at the end of branch link.

The 2.465-GHz LO_1 is used to monitor the phase error and alter the optical wavelengths. To demonstrate the extensibility of transferring more than one frequency signal, an extra LO_2 with the frequency of 900 MHz is added and combined with LO_1 at the central station. The LO input power at each MZM is set to

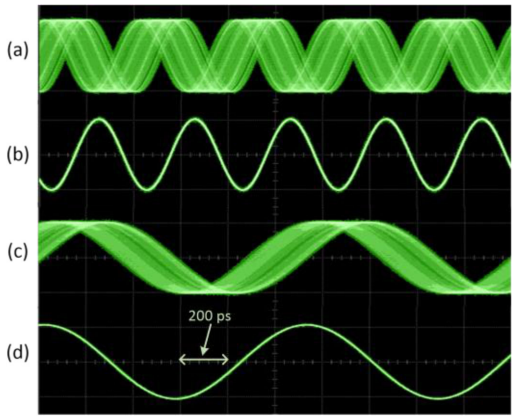

Fig. 4. Eye diagrams of the two recovered local oscillators at the end of the side-branch link after 30 minutes. (a), 2.465-GHz LO_1 without compensation; (b), 2.465-GHz LO_1 with compensation; (c), 900-MHz LO_2 without compensation; (d), 900-MHz LO_2 with compensation.

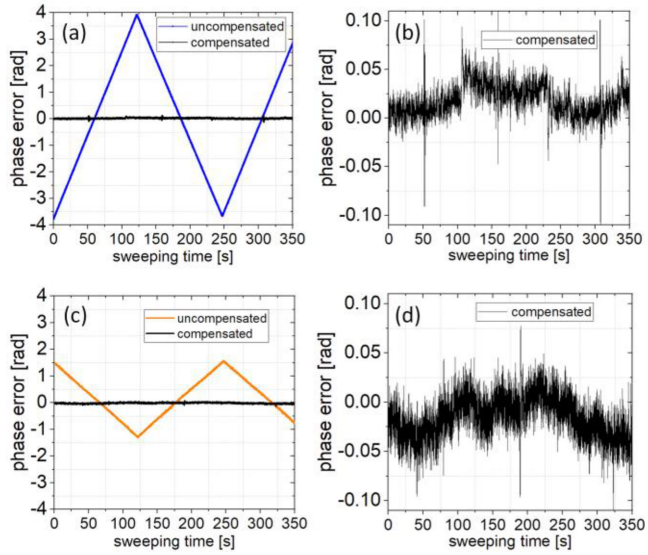

Fig. 5. Phase error (in radians) of the 2.465-GHz and 900-MHz LO with and without compensation, when the PODL sweeps its optical delay from 0 ps to 500 ps. (a), 2.465-GHz LO_1, compensated & uncompensated; (b), enlarged 2.465-GHz LO_1, compensated alone; (c), 900-MHz LO_2, compensated & uncompensated; (d), enlarged 900-MHz LO_2, compensated alone.

be around 15 dBm (i.e., the peak-to-peak voltage is around 3.5 V in the 50-Ω impedance system), after considering that the V_π of each MZM is 4.5 V, so as to achieve a loosely linear transfer function of the MZM. Both two LOs are recovered at the remote end of branch link.

A proportional-integral-derivative (PID) feedback algorithm is employed in the experiment, both in the main link and branch link. The AD8302 phase detector extracts the real-time phase difference between the original and returned LO_1. The output phase difference signal of AD8302 is fed into a STM32F103 microprocessor, then A/D converted, and the result is utilized by the PID algorithm also running on the microprocessor. The algorithm continuously adjusts the wavelength of the optical carrier several times within every second.

Fig. 4 illustrates the eye diagrams of the two transferred frequency signals at the end of the branch link. The temporal waveforms are sampled by a high-speed digital oscilloscope (Agilent DSO80604), accumulated for 30-minutes time. In Fig. 4(a), the 2.465-GHz LO_1 is directly transferred to the end of branch link without any wavelength tuning at central station or branch link, and the accumulated eye diagram shows drastic phase fluctuation in free-running situation after 30 minutes. In Fig. 4(b), wavelength-tuning-based phase locking is applied at both places, and a clear temporal waveform is obtained by the oscilloscope. Similarly, in Fig. 4(c), the 900-MHz LO_2 is combined with LO_1 and transmitted through the branch link, and the phase of the extra 900 MHz also varies a large amount without phase stabilization. As a contrast, the recovered phase of the 900-MHz signal keeps stabilized after phase locking, which is shown in Fig. 4(d).

The phase error at the end of side-branch link is also investigated quantitatively. A programmable optical delay line (PODL) is inserted into the 25-km side–branch link to simulate the fiber delay variations. The PODL is programmed to sweep its optical delay in 0∼500 ps range. The measured phase error fluctuations of the 2.465-GHz LO_1 and 900-MHz LO_2 are plotted in Fig. 5. As is shown by the blue zigzag curve in Fig. 5(a), the peak-to-peak phase error of the 2.465-GHz signal without compensation is as high as 7.62 rad, the value of which is in accordance with the 500-ps maximum delay sweeping range for the 2.465-GHz frequency. The phase fluctuation is expected to become larger if the PODL had a wider delay tunable range. As a comparison, the phase fluctuation of the stabilized 2.465-GHz LO is suppressed within only ±0.1 rad. A phase jitter suppression ratio of around 40 is achieved here. Similarly, in Fig. 5(c), the simultaneously delivered 900-MHz signal experiences a peak-to-peak phase fluctuation of about 2.8 rad under free-running condition, whereas the phase error with compensation is only within ±0.07 rad range. The occasional burrs in the compensated phase error, which is observed in Fig. 5(b) and Fig. 5(d), are caused by the sudden sweeping direction change of the PODL. The wavelength tuning speed of the WTL used in the experiment is at sub-Hertz level, and the burrs (i.e., sudden fiber delay change) can be better suppressed if using a WTL with higher tuning speed.

To mainly evaluate the long-term phase-stabilizing performance of both LOs, the frequency stability is measured and calculated by a frequency comparator (Keysight 53230a) in natural temperature changing environment in the laboratory. Fig. 6 shows the frequency stability of the 2.465-GHz LO_1 at the end of branch link, in terms of overlapping Allan Deviation (ADEV). For the short-term stability, the ADEV of 2.6×10^{-13} at 1 s averaging time is achieved with compensation. In the averaging time of 0∼100 s range, the ADEV of 2.465 GHz with and without compensation keeps very close, whereas the frequency stability starts to deteriorate after 100 s averaging time without compensation, and worsens to 1.2×10^{-13} at 10^4 s averaging time. However, when the proposed side-branch phase locking is applied, the recovered 2.465-GHz signal shows a

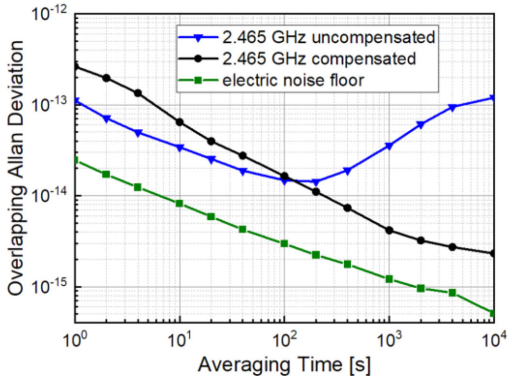

Fig. 6. Frequency stability (Allan Deviation, ADEV) of the 2.465-GHz LO_1 at the remote end of branch link.

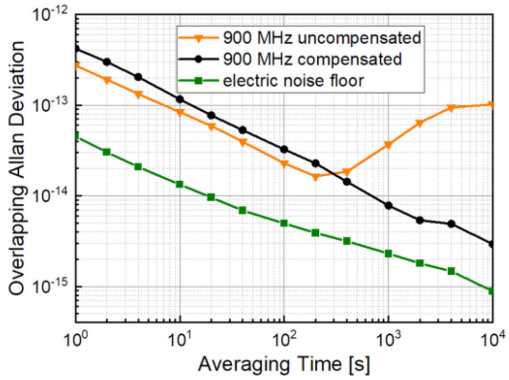

Fig. 7. Frequency stability (Allan Deviation, ADEV) of the 900-MHz LO_2 at the remote end of branch link.

long-term stability of 2.3×10^{-15} at 10^4 s averaging time, which indicates an optimization of two orders of magnitude compared to the free-running situation. Similarly, the frequency stability of the 900-MHz LO_2 is depicted in Fig. 7. When the side-branch phase locking is applied, the overlapping Allan Deviation shows 4.37×10^{-13} at 1 s and 2.65×10^{-15} at 10^4 s, respectively. As a contrast, the 10^4-s stability turns out to be 1.02×10^{-13} at 10^4 s averaging time, which also indicates a long-term stability optimization of two orders of magnitude. The relative intensity noise (RIN) of the WTL used in the experiment is at the 140 dBc/Hz level, and may deteriorate the output phase noise through the amplitude modulation to phase modulation (AM-PM) conversion process [34]. So a better phase noise (or short-term stability) performance can be expected by employing a laser source with lower RIN level. In addition, the wavelength tuning granularity (~1 pm minimum) of the WTL used in the experiment is believed to account for the slight deterioration of the short-term stability.

IV. Conclusion

In summary, we have proposed a phase-stabilized side-branch RoF link that simultaneously disseminates multiple frequencies to the end of the extensible branch link. We first analyze the requirements on extensibility of fiber-based sync systems, and demonstrate that the proposed side-branch link fully satisfies the extensibility requirements. Extensibility of the side-branch stable RoF link for synchronization is achieved for that on the one hand, the branch link can be installed on any intermediate point along the main link and works independently; on the other hand, any extra local oscillator can be easily added in the central station and automatically phase-stabilized in the same branch link. Experiment has demonstrated a frequency stability optimization of two orders of magnitude on both frequency signals. The side-branch multi-frequency dissemination scheme shows the potential of constructing a highly-extensible frequency synchronization network for modern time and frequency transfer applications, especially for system upgrading and capacity expansion. The future work on the extensible side-branch synchronized RoF link may involve time information transfer along with frequency and field experiment in the telecommunication optical networks.

Acknowledgment

The authors wish to thank the anonymous reviewers for their valuable suggestions.

References

[1] D. P. Venmani, O. L. Moult, F. Deletre, Y. Lagadec, and Y. Morlon, "On the role of network synchronization for future cellular networks: An operator's perspective," *IEEE Commun. Mag.*, vol. 54, no. 9, pp. 58–64, Sep. 2016.
[2] J. Zou, S. A. Sasu, J. Messenger, and J. P. Elbers, "Options for time-sensitive networking for 5G fronthaul," in *Proc. 45th Eur. Conf. Opt. Commun.*, 2019, pp. 1–3
[3] N. J. Gomes *et al.*, "Boosting 5G through ethernet: How evolved fronthaul can take next-generation mobile to the next level," *IEEE Veh. Technol. Mag.*, vol. 13, no. 1, pp. 74–84, Mar. 2018.
[4] A. Lometti, G. Cazzaniga, S. Frigerio, and L. Ronchetti, "Synchronization techniques in backhauling networks," in *Proc. 15th Int. Conf. Transparent Opt. Netw.*, 2013, pp. 1–6
[5] F. Wen and H. Wymeersch, "5G Synchronization, positioning, and mapping from diffuse multipath," *IEEE Wireless Commun. Lett.*, vol. 12, no. 1, pp. 43–47, Jan. 2021.
[6] 3GPP TR 22.862 V14.1.0 (2016-09), "3rd Generation Partnership Project; Technical Specification Group Services and System Aspects; Feasibility Study on New Services and Markets Technology Enablers for Critical Communications; Stage 1 (Release 14)," Sep. 2016.
[7] S. Johnson and O. A. Dobre, "Time and carrier frequency synchronization for coherent optical communication: Implementation considerations, measurements, and analysis," *IEEE Trans. Instrum. Meas.*, vol. 69, no. 8, pp. 5810–5820, Aug. 2020.
[8] R. K. Shiu *et al.*, "Optical signal processing for W-band radio-over-fiber system with tunable frequency response," *IEEE J. Sel. Top. Quant.*, vol. 27, no. 2, Mar./Apr. 2021, Art. no. 7600408.
[9] P. Ghelfi *et al.*, "A fully photonics-based coherent radar system," *Nature*, vol. 507, pp. 341–345, 2014.
[10] E. A. Kittlaus *et al.*, "A low-noise photonic heterodyne synthesizer and its application to millimeter-wave radar," *Nat. Commun.*, vol. 12, 2021, Art. no. 4397
[11] S. Lewis and M. Inggs, "Synchronization of coherent netted radar using white rabbit compared with one-way multichannel GPSDOs," *IEEE Trans. Aerosp. Electron. Syst.*, vol. 57, no. 3, pp. 1413–1422, Jun. 2021.
[12] F. Riehle, "Optical clock networks," *Nat. Photon*, vol. 11, pp. 25–31, 2017.
[13] V. Shrivastav, K. S. Lee, H. Wang, and H. Weatherspoon, "Globally synchronized time via datacenter networks," *IEEE ACM Trans. Netw.*, vol. 27, no. 4, pp. 1401–1416, Aug. 2019.
[14] D. J. Blumenthal *et al.*, "Frequency-Stabilized links for coherent WDM fiber interconnects in the datacenter," *J. Lightw. Technol.*, vol. 38, no. 13, pp. 3376–3386, Jul. 2020.
[15] H. Li, L. Han, R. Duan, and G. M. Garner, "Analysis of the synchronization requirements of 5G and corresponding solutions," *IEEE Commun. Standards Mag.*, vol. 1, no. 1, pp. 52–58, Mar. 2017.

[16] A. Yazar, S. D. Tusha, and H. Arslan, "6G Vision: An ultra-flexible perspective," *ITU J. Future Evolving Technol.*, vol. 1, no. 1, pp. 121–140, 2020.
[17] X. Du and H. Chen, "Security in wireless sensor networks," *IEEE Wireless Commun.*, vol. 15, no. 4, pp. 60–66, 2008.
[18] T. P. Krisher *et al.*, "Test of the isotropy of the one-way speed of light using hydrogen-maser frequency standards," *Phys. Rev.*, vol. 42, 1990, Art. no. 731
[19] L. S. Ma, P. Jungner, J. Ye, and J. L. Hall, "Delivering the same optical frequency at two places: Accurate cancellation of phase noise introduced by an optical fiber or other time-varying path," *Opt. Lett.*, vol. 19, no. 21, pp. 1777–1779, 1994.
[20] Y. He *et al.*, "Stable radio-frequency transfer over optical fiber by phase-conjugate frequency mixing," *Opt. Exp.*, vol. 21, no. 16, pp. 18754–18764, 2013.
[21] G. Marra *et al.*, "High-resolution microwave frequency transfer over an 86-km-long optical fiber network using a mode-locked laser," *Opt. Lett.*, vol. 36, no. 4, pp. 511–513, 2011.
[22] B. Wang *et al.*, "Precise and continuous time and frequency synchronisation at the 5×10-19 accuracy level," *Sci. Rep.*, vol. 2, 2012, Art. no. 556
[23] S. Zhang and J. Zhao, "Frequency comb-based multiple-access ultrastable frequency dissemination with 7 × 10-17 instability," *Opt. Lett.*, vol. 40, no. 1, pp. 37–40, 2015.
[24] H. Li, G. Wu, J. Zhang, J. Shen, and J. Chen, "Multi-access fiber-optic radio frequency transfer with passive phase noise compensation," *Opt. Lett.*, vol. 41, no. 24, pp. 5672–5675, 2016.
[25] G. Tong *et al.*, "Stable radio frequency dissemination in a multi-access link based on passive phase fluctuation cancellation," *Opt. Commun.*, vol. 423, pp. 53–56, 2018.
[26] C. Liu *et al.*, "GVD-insensitive stable radio frequency phase dissemination for arbitrary-access loop link," *Opt. Exp.*, vol. 24, no. 20. pp. 23376–23382, 2016.
[27] J. Shang *et al.*, "Stable frequency dissemination over multi-access fiber loop link with optical comb," *Opt. Exp.*, vol. 26, no. 26, pp. 33888–33894, 2018.
[28] H. Wang, X. Xue, S. Li, and X. Zheng, "All-optical arbitrary-point stable quadruple frequency dissemination with photonic microwave phase conjugation," *IEEE Photon. J*, vol. 10, no. 4, Aug. 2018, Art. no. 5501508
[29] S. W. Schediwy *et al.*, "High-precision optical-frequency dissemination on branching optical-fiber networks," *Opt. Lett.*, vol. 38, no. 15, pp. 2893–2896, 2013.
[30] L. Yu *et al.*, "WDM-based radio frequency dissemination in a tree-topology fiber optic network," *Opt. Exp.*, vol. 23, no. 15, pp. 19783–19792, 2015.
[31] C. Hu, B. Luo, W. Pan, L. Yan, and X. Zou, "Multipoint stable radio frequency long distance transmission over fiber based on tree topology, with user fairness and deployment flexibility," *Opt. Exp.*, vol. 28, no. 16, pp. 23874–23880, 2020.
[32] A. Zhang *et al.*, "Phase-stabilized delivery for multiple local oscillator signals via optical fiber," *IEEE Photon. J.*, vol. 6, no. 3, Jun. 2014, Art. no. 5500408
[33] V/ J. Urick, Jr., J. D. McKinney, and K. J. Williams, "Propagation effects," in *Fundamentals of Microwave Photonics*, Hoboken, NJ, USA: Wiley, 2015, pp. 184–190
[34] J. Taylor *et al.*, "Characterization of power-to-phase conversion in high-speed P-I-N photodiodes," *IEEE Photon. J.*, vol. 3, no. 1, pp. 140–151, Feb. 2011.